metals

MDPI

Article

Effects of Current Density and Bath Temperature on the Morphological and Anticorrosive Properties of Zn-Ni Alloys

Josiane D. Costa [1], Arthur F. Almeida [2], Renato A. C. Santana [2], Ana R. N. Campos [1], José A. M. Oliveira [2], José J. N. Alves [1], Tiago F. A. Santos [3,4], Antônio A. Silva [2], Shiva Prasad [1], Paulo C. S. Silva [2], Evelyn L. S. Souza [2], João M. P. Q. Delgado [5,*] and Antonio G. B. Lima [2]

1 Department of Chemical Engineering, Federal University of Campina Grande, Av. Aprígio Veloso, 882, Campina Grande 58429-970, Brazil; josianeeq@gmail.com (J.D.C.); ana.regina@professor.ufcg.edu.br (A.R.N.C.); jose.jailson@ufcg.edu.br (J.J.N.A.); prasad722@yahoo.com (S.P.)
2 Department of Mechanical Engineering, Federal University of Campina Grande, Av. Aprígio Veloso, 882, Campina Grande 58429-970, Brazil; arthur.filgueira@eq.ufcg.edu.br (A.F.A.); renato.alexandre@professor.ufcg.edu.br (R.A.C.S.); jmo.anderson@gmail.com (J.A.M.O.); antonio.almeida@ufcg.edu.br (A.A.S.); paulocesarsales@outlook.com (P.C.S.S.); evelynsouza@outlook.com (E.L.S.S.); antonio.gilson@ufcg.edu.br (A.G.B.L.)
3 Department of Mechanical Engineering, Federal University of Pernambuco, Av. da Arquitetura, s/n, Cidade Universitária, Recife 50740-550, Brazil; tiago.felipe@ufpe.br
4 Brazilian Institute for Material Joining and Coating Technologies (INTM), Federal University of Pernambuco, Recife 50670-901, Brazil
5 CONSTRUCT-LFC, Civil Engineering Department, Faculty of Engineering, University of Porto, 4200-465 Porto, Portugal
* Correspondence: jdelgado@fe.up.pt; Tel.: +351-225081404

Abstract: The effect of current density and bath temperature in the electroplating process on resistance to corrosion of Zn-Ni alloys was evaluated in this work. The electrolytic bath consisted of nickel sulfate, zinc sulfate, sodium sulfate, boric acid, and sodium citrate at pH 7.0. The current density was varied in the range 20–80 mA/cm^2 and the bath temperature in the range 30–60 °C. Increasing, independently, the current density or the bath temperature increased the nickel content in the obtained alloy, which affected the alloy microstructure, with a predominant γ phase and cauliflower-like morphology. The nickel content in the alloys was in the range 20–42%wt. A synergistic effect between the current density and bath temperature was observed from a design of experiments and response surface models. The maximum resistance to corrosion occurred for the alloy containing 42%wt. nickel. This alloy was obtained at upper levels of current density and bath temperature, presenting a corrosion potential of −0.789 V and polarization resistance of 4136 Ω.cm^2.

Keywords: electrodeposition; Zn-Ni alloy; corrosion resistance; design of experiments

check for updates

Citation: Costa, J.D.; Almeida, A.F.; Santana, R.A.C.; Campos, A.R.N.; Oliveira, J.A.M.; Alves, J.J.N.; Santos, T.F.A.; Silva, A.A.; Prasad, S.; Silva, P.C.S.; et al. Effects of Current Density and Bath Temperature on the Morphological and Anticorrosive Properties of Zn-Ni Alloys. *Metals* **2023**, *13*, 1808. https://doi.org/10.3390/met13111808

Academic Editor: Frank Czerwinski

Received: 21 September 2023
Revised: 19 October 2023
Accepted: 23 October 2023
Published: 26 October 2023

Copyright: © 2023 by the authors. Licensee MDPI, Basel, Switzerland. This article is an open access article distributed under the terms and conditions of the Creative Commons Attribution (CC BY) license (https://creativecommons.org/licenses/by/4.0/).

1. Introduction

Electroplating is a metal alloy manufacturing process widely used due to its simplicity and low cost compared with other techniques, as well as being applied to objects with different geometries [1,2]. Cadmium coatings obtained by electrodeposition are used to increase the corrosion resistance of different materials in a wide range of components and parts in many industrial applications [3]. However, cadmium has major drawbacks due to its high toxicity [4,5]. An alternative for replacing cadmium coatings is zinc coatings obtained by the electroplating process [3,6–13]. Zinc coatings are widely used in the industry, mainly applied as a corrosion-resistant coating [10,14]. Zinc alloys have substituted pure zinc due to their properties being superior to those of pure metal [8,15,16].

Zinc-forming alloys with elements of the iron group (iron, cobalt, and nickel) have been investigated due to their high resistance to corrosion and low toxicity [17–22]. The least noble element, in this case, zinc, deposits more preferentially than the noblest element,

in this case, the elements of the iron group [23], in the so-named anomalous co-deposition process [6,9,24–26]. It has been observed that normal co-deposition can occur in addition to anomalous co-deposition depending on the electrodeposition's operational condition, especially the pH [13,26,27]. The mechanism that occurs in the deposition of the Zn-Ni alloy has not yet been fully clarified, with the hydroxide suppression mechanism (HSM) being the most accepted. Several mechanisms have been proposed and described in the literature, thus showing the current interest in obtaining Zn-Ni alloys [9,13,23,24,28].

The addition of metals such as iron, nickel, or cobalt to a zinc alloy causes a modification of the corrosion potential of the deposit, compared with that of pure zinc. The alloy becomes slightly nobler than pure zinc, and therefore, the corrosion rate of the deposit is slower. As the deposit has the function of being sacrificed to protect the substrate, it means that for the same deposit thickness, the zinc alloy has the advantage of protecting the substrate for a longer period than the conventional zinc [29,30].

The electroplating process to produce Zn-Ni coatings has been used and improved for decades due to both the low-cost manufacturing process and the corrosion resistance of the alloy, adequate for various applications. Zn-Ni alloys with Ni content in the range of 12–14%wt more resistance to corrosion than pure zinc have been reported in the literature [10,13,31]. On the other hand, some reports suggest that increasing the Ni content in the alloys generates internal stresses and microcracks, and as a consequence, a higher level of nickel may not improve the coating protection against corrosion [3,32,33]. In fact, depending on the electrodeposition conditions as well as the bath composition, it is possible to produce coatings with higher Ni content without microcracks, resulting a high resistance to corrosion protection. Unfortunately, a few studies describe the electrodeposition process of Zn-Ni alloys for producing high Ni content alloy, as stated by Roventi et al. [24]. The control of the bath pH, which can be acidic or basic, with and without cyanides, is fundamental for the electrodeposition of the Zn-Ni alloy. Many works are carried out in acid baths owing to a high cathodic efficiency. On the other hand, neutral or basic baths reduce the risk of hydrogen embrittlement and generate coatings with better nickel distribution [3,6,10,13–15,34–36]. In addition to pH, the complexing agents play an important role to produce coatings of good quality. There is a wide variety of complexing agents, among them tartrate, acetate, citrate, glycine, dimethyl hydantoin, triethanolamine, and EDTA, which are the most used complexing agents [9,10,14,34,36,37].

The success of the electrodeposition process to produce Zn-Ni coatings depends on many operational parameters such as the pH, current density, temperature, agitation, and bath composition. Most studies investigate the effects of operational parameters on the electrodeposition of Zn-Ni coatings following a traditional experimental methodology in which one parameter is varied while the others are kept constant [3,9,24,31,38]. This approach is time-consuming, unable to detect interactions between parameters leading to erroneous conclusions, and inappropriate for optimization purposes [39]. The experimental study may be simplified by using experiment optimization techniques such as factorial design. The advantages of factorial design compared with univariate methods are the reduction in the number of experimental runs, statistical reliability in the obtained results, and the possibility of evaluating synergies between the variables, which results in improvement of the yield and overall performance of the process [40]. Factorial design is often associated with the response surface methodology (RSM) as an optimization tool [40–43].

This work aimed to evaluate the influence of current density and bath temperature on the electrodeposition process for producing Zn-Ni coatings with high Ni content. The novelty was the use of a neutral electrolytic bath and a different complexing agent composed of sodium citrate and boric acid to favor the nickel deposition leading to a high Ni content alloy. Zn-Ni alloys with 20–42%wt. Ni content, different morphologies, and consequent different corrosion resistances resulted in different operational conditions in the electrodeposition process.

2. Materials and Methods

A design of experiments was performed to define the operational conditions of experimental runs, while the electrolytic bath, substrate preparation, electrodeposition, corrosion tests, and alloy characterization were performed as described as follows.

2.1. Design of Experiments

The design of experiments (DOE) associated with the response surface methodology (RSM) is used to quantify the influence of the input variables on response variables performing a minimum number of experiments while guaranteeing the accuracy of the results. A complete 2^2 factorial design with two central points was used to set the experiments and associated with the response surface methodology (RMS) to find the optimal current density and bath temperature (input variables Xi's) that maximizes the Ni content (response variable Y) in the Zn-Ni alloy. The experiments were carried out in triplicate. Table 1 shows the real and coded levels of the input variables in the design of experiments.

Table 1. Input variables and real and coded levels used in the response surface design.

Factors		Code		
		−1	**0**	**+1**
Current density (mA/cm^2)	X1	20	50	80
Bath temperature (°C)	X2	30	45	60

The second-order model considering the interaction term used in this work is given by Equation (1). Statistical analyses were performed using Statistica© version 8.0 software.

$$Y = \beta_0 + \beta_1 X_1 + \beta_2 X_2 + \beta_{12} X_1 X_2 \quad (1)$$

where βi and βjk are regression coefficients.

2.2. Preparation of the Electrolytic Bath

The electrolytic bath was prepared at a room temperature of 25 ± 2 °C. Distillated water and reagents with analytical purity were used to preparate the electrolytic bath with the following composition: boric acid (0.2 mol/L, Neon, São Paulo, Brazil), sodium citrate (0.2 mol/L Neon, São Paulo, Brazil), sodium sulfate (0.2 mol/L, Neon, São Paulo, Brazil), nickel sulfate (0.1 mol/L, Neon, São Paulo, Brazil), and zinc sulfate (0.1 mol/L Neon, São Paulo, Brazil). The electrolytic bath pH was adjusted to 7.0 by adding concentrated sulfuric acid (H_2SO_4, Vetec, Rio Janeiro, Brazil) or sodium hydroxide (NaOH, Vetec, Rio Janeiro, Brazil).

2.3. Substrate Preparation

Copper plates (substrate) with a deposition surface area of 8 cm^2 were used as a working electrode. The substrate was polished with sandpaper of different sizes in sequence from the thickest to the thinnest: 400, 600, and 1200 mesh. A chemical treatment was carried out by washing the electrode in a diluted solution of sodium hydroxide (NaOH, 10%) and sulfuric acid (H_2SO_4, 1%) to remove contaminants remaining from the mechanical polishing process. Finally, the substrate was washed with distilled water and dried in an oven.

2.4. Electrodeposition

The electrodeposition process was carried out under galvanostatic control in a conventional two-electrode deposition system. In this system, the cathode (copper substrate) was in the center of anode, a platinum cylindrical mesh, which was immersed in the electrolytic bath. A potentiostat MQPG-01 was used to set up and control the current density. An MTA Kutesz MD2 thermostat controlled the system temperature. After the electrodeposition step, the coated substrate was rinsed, dried in an oven, and cooled in a desiccator.

2.5. Material Characterization

The morphological characterization of the Zn-Ni alloys was performed by scanning electron microscopy (SEM) using a TESCAN microscope VEGA 3SBH (Kohoutovice, Czech Republic). Surface images with 3000× and 6000× magnification of the samples, without suffering any previous treatment, such as polishing or superficial chemical attack, were obtained.

The chemical composition was determined by the energy-dispersive X-ray (EDX) technique using an EDX-720 Shimadzu X-ray dispersive energy spectrometer. X-ray diffraction (XRD) tests were used to evaluate the alloy's microstructure using a Shimadzu diffractometer XRD-6100, with Cu Kα radiation (k = 1.54 Å) at 30 kV and 30 mA, a step size of 0.02, and a dwell time of 1 s. The scan range was from 20° to 90°.

2.6. Corrosion Tests

Potentiodynamic polarization (PP) and electrochemical impedance spectroscopy (EIS) techniques were used to assess the corrosion resistance of the Zn-Ni alloy in a corrosive medium containing chloride ions (NaCl, 3.5%). The tests started with stabilization of 60 min at room temperature (25 ± 2 °C) in the open circuit potential (OCP). The corrosion tests were carried out in an adapted conventional system composed of three electrodes, with the copper substrate coated with the Zn-Ni alloy acting as the working electrode, a platinum sheet as the counter electrode, and the saturated calomel electrode (SCE) used as a reference. The working electrode area exposed to the corrosion tests was 1 cm^2.

The polarization curves were obtained with a scan rate of 1 mVs^{-1} over a scan range of ±0.3 V from the OCP, using an Autolab PG STATE 302N potentiostat/galvanostat connected to a computer using NOVA 1.11 software.

The EIS tests were performed with a frequency range from 10 kHz to 0.004 Hz and an amplitude of 0.01 V. All corrosion experiments were carried out in triplicate at room temperature (25 ± 2 °C).

3. Results

Table 2 shows the matrix of the experimental design 2^2, the results of corrosion (corrosion potential, E_{corr}; corrosion current density, i_{corr}; and polarization resistance, Rp), and the chemical composition (Ni and Zn contents).

Table 2. Matrix of factorial design 2^2 for Zn-Ni alloy.

Run	J (mA/cm^2)	T (°C)	E_{corr} (V)	I_{corr} ($\mu A/cm^2$)	Rp ($k\Omega.cm^2$)	Ni %wt.	Zn %wt.
1	−(20)	−(30)	−1.2340	84.584	0.4519	22	78
2	+(80)	−(30)	−0.990	59.966	1.2291	26	74
3	−(20)	+(60)	−0.929	77.127	0.5732	23	77
4	+(80)	+(60)	−0.789	6.848	4.1363	42	58
5	0 (50)	0 (45)	−0.992	15.306	1.9390	27	73
6	0 (50)	0 (45)	−0.983	14.020	2.1380	28	72

3.1. Chemical Composition

The effect of current density and bath temperature on the coatings' chemical composition was evaluated and optimized using RSM, which provides information on the effects of the variables separately as well as the synergistic effects between the variables in the analyzed responses [39]. The RSM technique has been used as optimization tool in different research areas and has grown in recent years [44–51].

The response surface of the influence of the current density and the bath temperature on the nickel content in the obtained coating is shown in Figure 1. It is worth mentioning that different from the reports in the literature, all coatings in this work were obtained at a neutral pH using sodium citrate as a complexing agent. The complexing agent has the function of stabilizing the bath in addition to promoting nickel deposition.

As the current density was varied, the chemical composition of the coatings changed. Increasing the current density increased the Ni content in the coating, as shown in Figure 1. The experimental results are represented by the blue circles on the response surface. Increasing the current density increased the cathode polarization due to the nickel complex's formation with sodium citrate. It reduced the $Zn(OH)_2$ barrier formed on the cathode surface, favoring the reduction in nickel in the coatings. This layer/barrier was related to the hydroxide suppression mechanism (HSM).

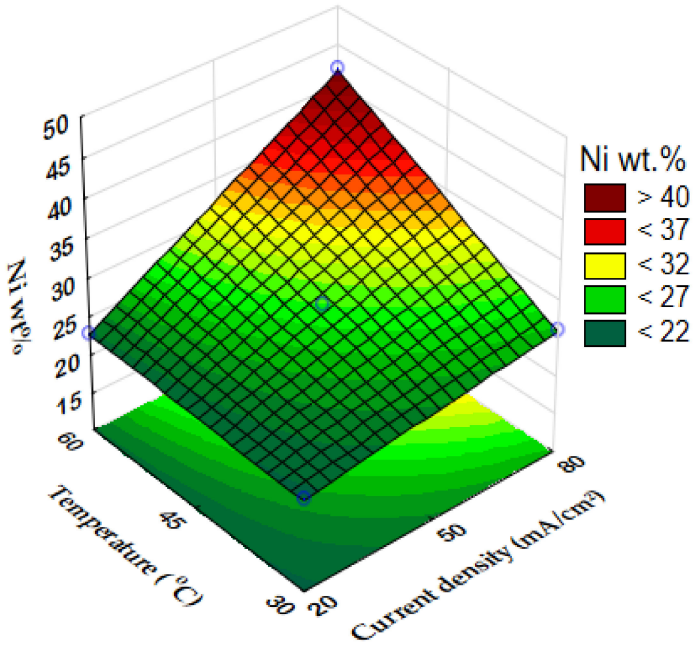


Figure 1. Response surface for nickel content in Zn-Ni alloy as a function of the current density and bath temperature.

The Ni content in all coatings was higher than 20%wt., reaching 42%wt. with a current density of 80 mA/cm^2. Dark and powdery coatings with little adherence were obtained with a current density above 80 mA/cm^2. Hegde et al. [29] reported the electrodeposition of Zi-Ni alloy in an acid bath (pH = 3.5) using different current densities, with an average Ni content of 22%wt., lower than that obtained in the present study. Zhongbao et al. [10] obtained a Zn-Ni alloy in an alkaline bath using DMH as a complexing agent and observed that increasing the current density increased the Ni content in the coating, similar to the findings in the present work.

Figure 2 shows that increasing the bath temperature increased the Ni content in the coating and, consequently, decreased the Zn content in the deposit. The temperature increase affected the ion mobility and the characteristics of the double layer at the electrode/electrolyte interface, by the exchange of zinc ions with nickel ions, which favored the reduction in nickel in the coating. Pagotto et al. [7] reported that increasing the bath temperature increased the nickel content in the coating. Qiao et al. [52] studied the influence of temperature on the electrodeposition of Zn-Ni alloys and concluded that increasing the bath temperature increased the cathodic potential. It was also reported that at low current densities, the film formed was rich in zinc, while at high current densities, it was rich in nickel. Zhongbao et al. [10] observed that high temperatures favored the co-deposition of the Zn-Ní alloy, and in addition, the deposition kinetics became more efficient.

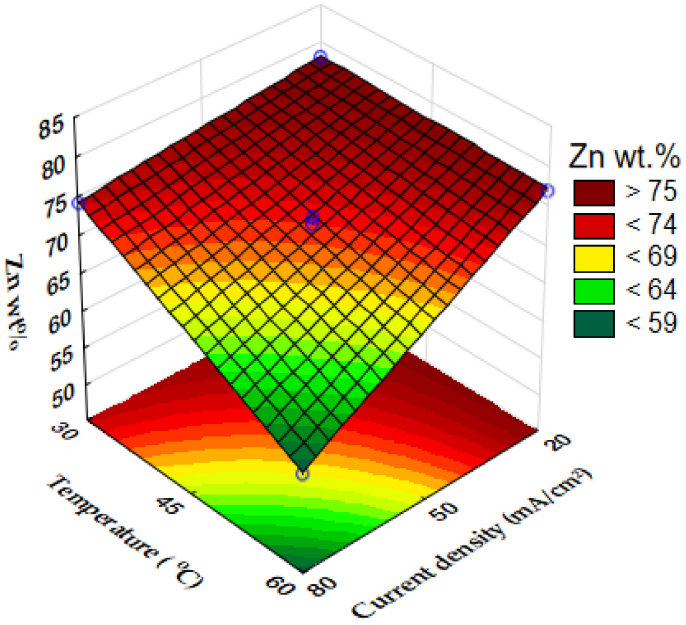


Figure 2. Response surface for zinc weight content as a function of current density and bath temperature of Zn-Ni alloy coatings.

Byk et al. [13] observed that increasing the current density favored the reduction in nickel in the coatings due to the decrease in zinc ions and the increase in nickel ions in the double layer. Thus, the deposition mechanism could change from anomalous to normal co-deposition depending on the operating conditions of the electrodeposition process. A synergy was observed between the effects of current density and bath temperature. As they increased, the nickel content increased in the coatings. Anomalous-type deposition occurred at low current density and low temperatures, while normal-type co-deposition occurred with the increase in the current density and temperature as the quantity of the noblest element was increased.

The synergy effect was proven with the use of the response surface methodology associated with the experimental design. The nickel and zinc contents can be predicted by using Equations (2) and (3), a first-order linear model, obtained from experimental data and RSM with 95% confidence. The significant terms are highlighted in bold in Equations (2) and (3).

$$Ni\ \%wt. = 28 + 5.75 \times X1 + 4.25 \times X2 + 3.75 \times X1 * X2 \quad (2)$$

$$Zn\ \%wt. = 100 - Ni\ \%wt. \quad (3)$$

where $X1$ is the current density, $X2$ is the temperature, and $X1 * X2$ is the interaction between the current density and bath temperature.

Analysis of variance (ANOVA) was used to assess the synergy effect between the variables, with a 95% confidence level ($p < 0.05$), using F and p tests. Table 3 shows p-values lower than 0.05 for both variables, as well as for the interaction between the current density and the temperature. The ANOVA results in Table 3 demonstrate that the statistical model was significant and predictive for $p < 0.05$. The model fitting was also expressed by the determination coefficient (R^2), equal to 0.99 for nickel and zinc contents. A coefficient of determination values above 95% indicates that the proposed models significantly represented the experimental results. Thus, ANOVA and the determination coefficient demonstrated the statistical significance of the model, justifying the use of a first-order model. The Pareto graph shows the magnitude of the significance of each variable, confirming that the syn-

ergy effect influenced the electrodeposition process and especially the nickel content in the coating (Figure 3).

Table 3. Results of analysis of variance (ANOVA) for the Ni and Zn weight content of the Zn-Ni alloy.

Factors	Quadratic Sum	Degree of Freedom	Quadratic Average	F	*p*
Sodium tungstate (M)	132.2500	1	132.2500	211.6000	0.004693
Nickel sulfate (M)	72.2500	1	72.2500	115.6000	0.008540
Iteration	56.2500	1	56.2500	90.0000	0.010929
Error	1.2500	2	0.6250		
Total quadratic sum	262.0000	5			

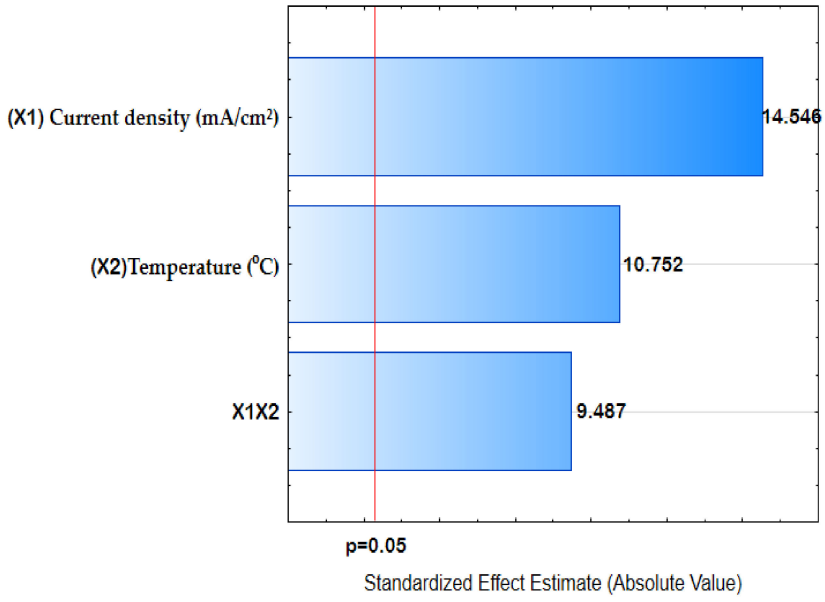
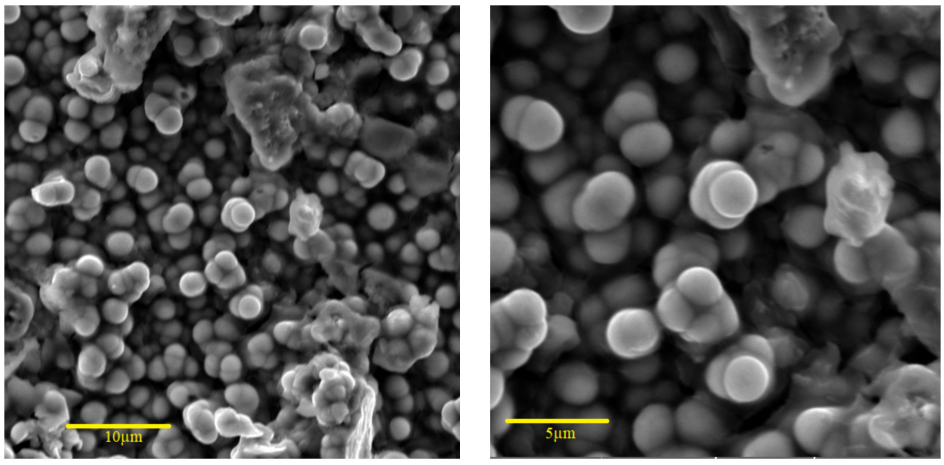


Figure 3. Pareto graph for nickel content in Zn-Ni alloy.

3.2. Surface Morphology

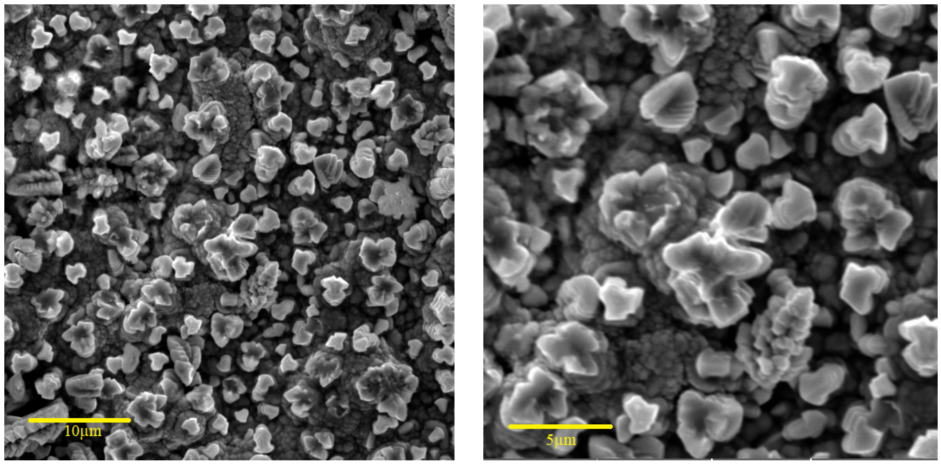
The scanning electron microscopy in the gray color of the Zn-Ni coatings containing the lowest and highest nickel content is shown in Figures 4 and 5, respectively. Both were porous and not shiny; however, the surface morphology was modified, increasing the current density and temperature. The increase in these variables caused a modification in the microstructure through the refinement of the grains [20,53]. It can be observed that the increase in the nickel content in the coating modified the morphology from nodular to cauliflower, as can be seen by comparing Figure 4 with Figure 5. Hammami et al. [54] associated the cauliflower structure to the rapid growth of some particles. Ruiqian et al. [26] obtained a morphology similar to bunches of flowers. With the modification in the morphology, there was an increase in the surface area that was rich in nickel. The same morphological structure was observed by Constantin [55] and Zheng et al. [56].

XRD analyses performed for the coatings with the lowest and highest Ni content are shown in Figure 6. The most intense peaks corresponded to the γ-Ni5Zn_{21} phase, and the less intense peaks corresponded to the pure zinc phase. The γ phase of the Zn-Ni alloy exhibited a centered body cubic structure. The Ni content in every sample was higher than 20%wt., and only the γ phase predominant was observed. Similar results were reported by Mosavat et al. [34,57] and Abou-Krisha et al. [58]. A preferential orientation was observed in plans (411), similar to the results reported in the literature [10,59]. It was also observed that the alloy with the highest nickel content, the one from Exp. 4, presented peaks with higher intensity than that from Exp. 1. The coatings obtained had an average thickness of 5.1 μm.



(**a**) (**b**)

Figure 4. Scanning electron microscopy for the Zn_{78}-Ni_{22} alloy (test 1) with amplification of (**a**) 3000× and (**b**) 6000×.



(**a**) (**b**)

Figure 5. Scanning electron microscopy Zn_{58}-Ni_{42} alloy (test 4) with amplification of (**a**) 3000× and (**b**) 6000×.

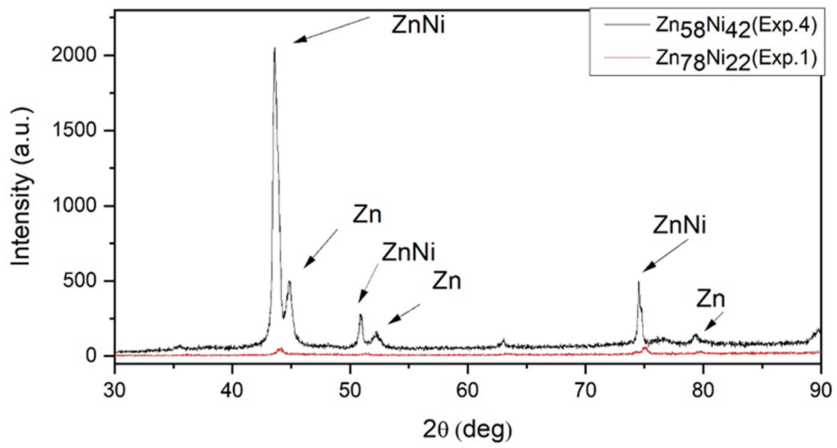


Figure 6. XRD patterns of the $Zn_{58}Ni_{42}$ and $Zn_{78}Ni_{22}$ alloys.

3.3. Corrosion Measurements

To assess the corrosion resistance of the Zn-Ni alloys in a corrosive medium containing chloride ions (NaCl, 3.5%), potentiodynamic polarization (PP) measurements were taken to

obtain the electrochemical parameters, corrosion potential (E_{corr}), current corrosion (i_{corr}), and resistance to polarization (Rp) using the Tafel straight-line extrapolation technique. As can be seen from Table 2, the highest corrosion resistance was for the alloy from experiment 4, which was the alloy with the highest nickel content. It has been reported in the literature that the increase in the nickel content in the coating increases the corrosion resistance of the alloy [10,26,28,29]. The response surface of the effect of current density and temperature on corrosion potential is shown in Figure 7. As the nickel content increased, the corrosion potential shifted to more positive values, from −1.23 V to −0.789 V, which were more positive than the zinc potential (around −1.37 V). Zn-Ni alloys with corrosion potential close to that of zinc have been reported in the literature [60–63], as well as results similar to those of this study, as reported by Byk et al. [13] for alloys with a nickel content above 50%wt. The corrosion potential shifting could be related to the formation of a nickel-rich layer associated with the presence of the γ phase, which caused the surface to be more noble, favoring the increase in corrosion resistance.

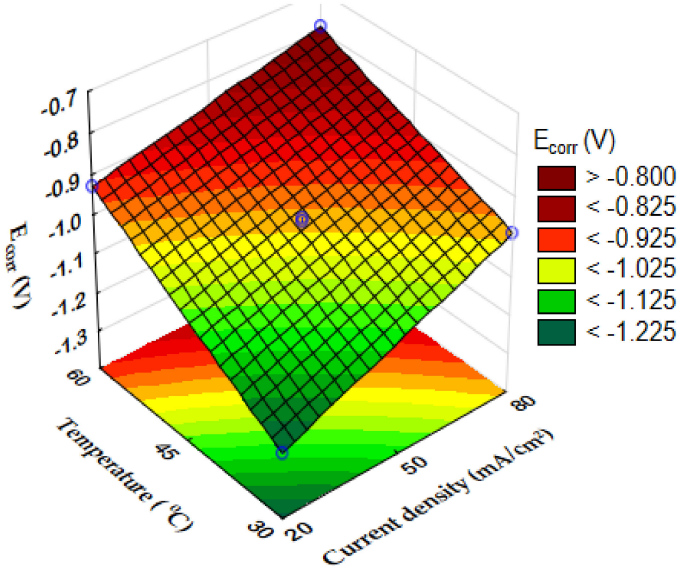


Figure 7. Response surface of the corrosion potential of a Zn-Ni alloy as a function of current density and temperature in the electrodeposition.

Increasing the current density and bath temperature increased the polarization resistance, as shown by the response surface of the polarization resistance in Figure 8, and decreased the corrosion current, as shown by the polarization curves in Figure 9. The highest resistance to polarization was approximately 4136 $\Omega.cm^2$, which was higher than those reported in the literature [28,29]. Tafreshi et al. [64] related the increase in the corrosion resistance to the compact cauliflower morphology. Tozar et al. [65] evaluated the corrosion resistance of Zn-Ni alloys obtained using sodium citrate and boric acid as a complexing agent, varying the current density, at a constant temperature of 30 °C and pH 3. Zinc-rich coatings and lower corrosion resistances than those obtained in this work were reported.

The different corrosion potential for different curves shown in Figure 9 is due to the alloy composition. As the Ni content in the alloy increased, so did the corrosion potential, as can be seen from the potentiodynamic polarization curves in Figure 9. The curves also reveal that both coatings showed active dissolution characteristics without passivation behavior, that is, they were sacrifice coatings for the protection of the substrate; similar behavior was reported by Sriraman et al. [66]. The corrosion potential of coatings rich in zinc was closer to that of pure zinc; thus, the alloy was less resistant to corrosion.

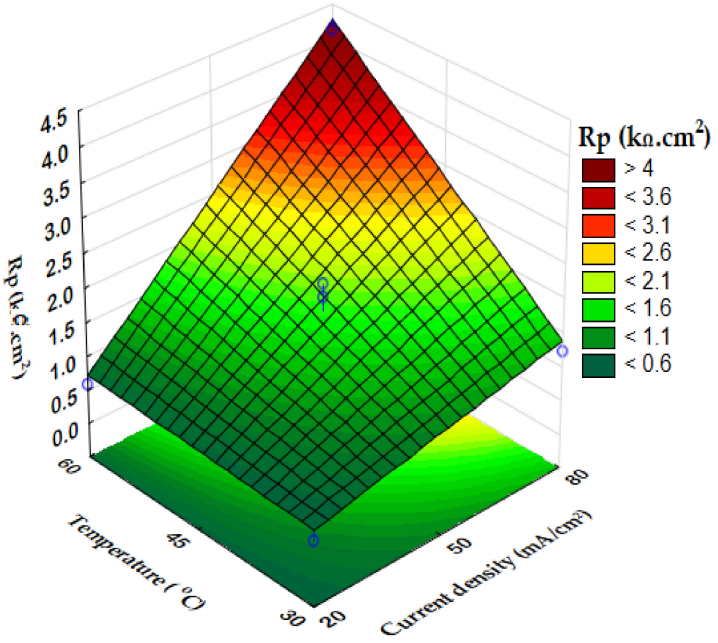


Figure 8. Response surface of the polarization resistance of a Zn-Ni alloy as a function of current density and temperature in the electrodeposition.

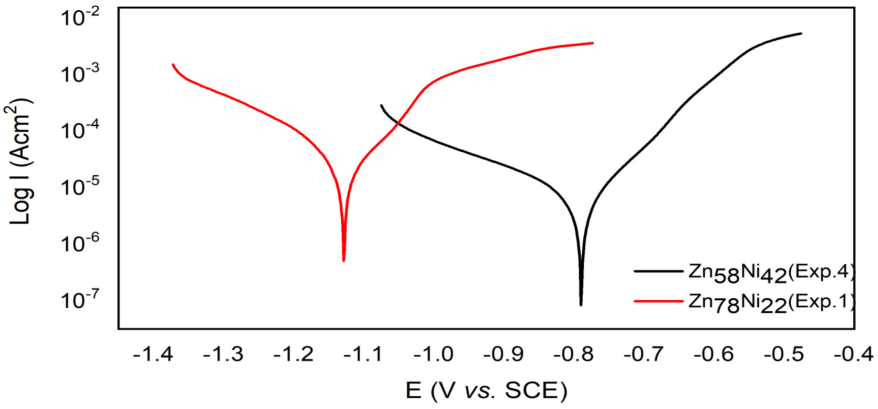


Figure 9. Polarization curves of $Zn_{58}Ni_{42}$ and $Zn_{78}Ni_{22}$ alloys.

Electrochemical impedance spectroscopy (EIS) measurements were performed in open circuit potential to obtain detailed information on the corrosion resistance of Zn-Ni alloys. The Nyquist diagrams for the coatings richest in zinc (experiment 1) and richest in nickel (experiment 4) are shown in Figure 10. Semicircles can be seen, which characterize the phenomenon of charge transfer, thus confirming the polarization curve results, where there is no formation of stable passivation. The semicircle for the coating richest in nickel (experiment 4), the optimum experiment among the runs, has a diameter three times larger than that for the coating richest in zinc (experiment 1).

Equivalent electrical circuit analysis is a well-established method for interpreting EIS spectra and extracting more details from the solution/coating interaction. The equivalent electrical circuit used in this work is shown in Figure 11. With this circuit, it is possible to characterize the effect of corrosion at the metal interface, which can be obtained by increasing the resistance to charge transfer. A similar circuit was used by Bahadormanesh et al. [38] to adjust the spectra, similar to this work. A non-ideal capacitor QPE can replace the CPE. To calculate the QPE value, Equation (4) was used:

$$Z_{QPE} = 1/Q\,(j\omega)^{\alpha} \quad (4)$$

where j is the square root of -1, ω is the angular frequency, and Q and α are the parameters to be adjusted.

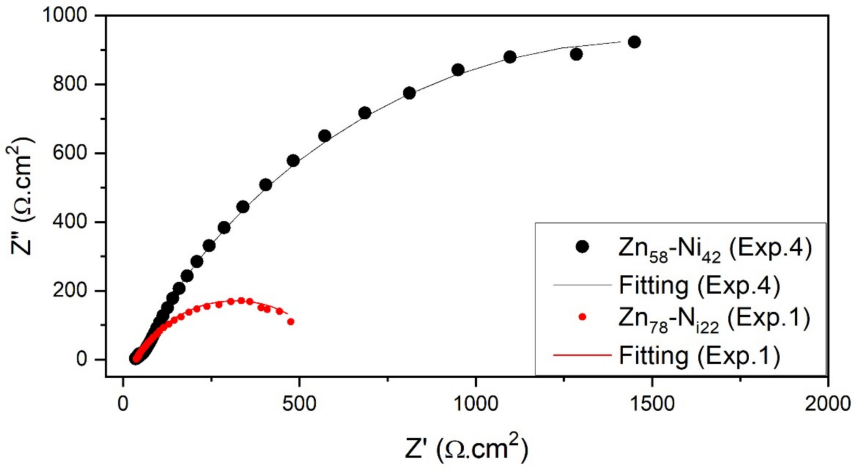


Figure 10. Nyquist diagram for the Zn_{78}-Ni_{22} and Zn_{58}-Ni_{42} alloys.

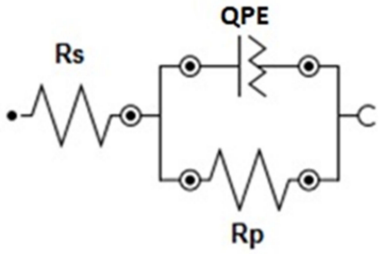


Figure 11. Equivalent electric circuit used for fitting the EIS experimental results.

It has been reported that these parameters are used to adjust the equivalent electrical circuit using a non-ideal capacitor [67–70]. According to Mishra et al. [68], for a perfect capacitor, the α value is equal to 1. However, this value is lower than 1 due to the roughness of the coating or its inhomogeneity; thus, the behavior of a non-ideal capacitor is observed [68–72]. The values of the parameters Rs, Rp, and QPE, obtained from the equivalent electrical circuit, are shown in Table 4.

Table 4. Adjusted data extracted from the equivalent circuit of $Zn_{78}Ni_{22}$ and $Zn_{58}Ni_{42}$ alloys in 3.5% NaCl solution.

Coating	Rs (Ω cm²)	Rp (Ω cm²)	Y (S s^{α} cm^{-2})	α
$Zn_{78}Ni_{22}$ (Exp. 1)	37.62	564	0.00029	0.70
$Zn_{58}Ni_{42}$ (Exp. 4)	38.95	2924	0.00017	0.72

Table 4 shows that the resistance of the solution (Rs) was almost the same in both cases since the same solution and cell configuration were used for every experiment. The Rp values indicate that the increase in the Ni content in the alloy increased the corrosion resistance and modified the morphology from nodular to cauliflower with a predominance of the γ phase, which also contributed to increase the corrosion resistant of the alloy.

4. Conclusions

Zn-Ni coatings were successfully obtained in a neutral bath and using sodium citrate as a complexing agent. The increase in the current density and bath temperature increased the nickel content in the coatings and modified the morphology of the alloy with a predominance of the γ phase. The nickel content of every alloy was above 20%wt., reaching

42%wt. The synergy effect between the variables was confirmed using the response surface methodology. Increasing the current density and bath temperature increased the corrosion resistance of the alloy. At the optimal experimental conditions, the corrosion potential reached −0.789 V, and the polarization resistance was 4136 $\Omega.cm^2$. The optimal operational conditions were a current density of 80 mA/cm^2 and a bath temperature of 60 °C.

Author Contributions: Conceptualization: J.D.C. and R.A.C.S.; formal analysis: J.D.C., E.L.S.S., J.A.M.O., T.F.A.S. and R.A.C.S.; funding acquisition: J.D.C., E.L.S.S., R.A.C.S., J.M.P.Q.D. and A.G.B.L.; investigation: J.D.C. and J.A.M.O.; resources: R.A.C.S., A.R.N.C., A.A.S. and S.P.; supervision: R.A.C.S., S.P. and J.J.N.A.; validation: J.D.C., J.A.M.O., J.M.P.Q.D. and A.G.B.L.; writing—original draft: J.D.C., R.A.C.S. and P.C.S.S.; writing—review and editing: P.C.S.S., A.F.A., J.J.N.A., J.M.P.Q.D. and A.G.B.L. All authors have read and agreed to the published version of the manuscript.

Funding: This research was funded by Brazilian National Council for Scientific and Technological Development (CNPq) for the scholarship PQ-1A and for the scholarship PQ-DT Level 2, grant number 308251/2020-2; the Paraíba State Research Support Foundation (FAPESQ-PB); and the Brazilian Coordination for the Improvement of Higher Education Personnel (CAPES) for the doctoral scholarship to Paulo César Sales da Silva and for the post-doctoral scholarship to Josiane Dantas Costa. In addition, this work was a result of the project "BlueHouseSim", with reference 2022.06841.PTDC, funded by national funds (PIDDAC) through FCT/MCTES. Furthermore, this work was financially supported by Base Funding-UIDB/04708/2020 and Programmatic Funding-UIDP/04708/2020 of the CONSTRUCT-Instituto de I&D em Estruturas e Construções-funded by national funds through the FCT/MCTES (PIDDAC) and by FCT—Fundação para a Ciência e a Tecnologia through the individual Scientific Employment Stimulus 2020.00828.CEECIND.

Data Availability Statement: Data are contained within the article.

Acknowledgments: We are grateful to the Laboratory of Microscopy of the Department of Mechanical Engineering (Federal University of Campina Grande) for technical support.

Conflicts of Interest: The authors declare no conflict of interests.

References

1. Torabinejad, V.; Aliofkhazraei, M.; Assareh, S.; Allahyarzadeh, M.H.; Rouhaghdam, A.S. Electrodeposition of Ni-Fe Alloys, Composites, and Nano Coatings–A Review. *J. Alloys Compd.* **2017**, *691*, 841–859. [CrossRef]
2. He, J.; Li, D.W.; He, F.L.; Liu, Y.Y.; Liu, Y.L.; Zhang, C.Y.; Ren, F.; Ye, Y.J.; Deng, X.D.; Yin, D.C. A Study of Degradation Behaviour and Biocompatibility of Zn—Fe Alloy Prepared by Electrodeposition. *Mater. Sci. Eng. C* **2020**, *117*, 111295. [CrossRef] [PubMed]
3. Conde, A.; Arenas, M.A.; de Damborenea, J.J. Electrodeposition of Zn–Ni Coatings as Cd Replacement for Corrosion Protection of High Strength Steel. *Corros. Sci.* **2011**, *53*, 1489–1497. [CrossRef]
4. Wang, Y.; Mandal, A.K.; Son, Y.-O.; Pratheeshkumar, P.; Wise, J.T.F.; Wang, L.; Zhang, Z.; Shi, X.; Chen, Z. Roles of ROS, Nrf2, and Autophagy in Cadmium-Carcinogenesis and Its Prevention by Sulforaphane. *Toxicol. Appl. Pharmacol.* **2018**, *353*, 23–30. [CrossRef] [PubMed]
5. Wang, Z.; Yang, C. Metal Carcinogen Exposure Induces Cancer Stem Cell-like Property through Epigenetic Reprograming: A Novel Mechanism of Metal Carcinogenesis. *Semin. Cancer Biol.* **2019**, *57*, 95–104. [CrossRef] [PubMed]
6. Srivastava, C.; Ghosh, S.K.; Rajak, S.; Sahu, A.K.; Tewari, R.; Kain, V.; Dey, G.K. Effect of PH on Anomalous Co-Deposition and Current Efficiency during Electrodeposition of Ni-Zn-P Alloys. *Surf. Coat. Technol.* **2017**, *313*, 8–16. [CrossRef]
7. Pagotto, S.O.; de Alvarenga Freire, C.M.; Ballester, M. Zn–Ni Alloy Deposits Obtained by Continuous and Pulsed Electrodeposition Processes. *Surf. Coat. Technol.* **1999**, *122*, 10–13. [CrossRef]
8. Bahadormanesh, B.; Ghorbani, M. Ni-P/Zn-Ni Compositionally Modulated Multilayer Coatings—Part 1: Electrodeposition and Growth Mechanism, Composition, Morphology, Roughness and Structure. *Appl. Surf. Sci.* **2018**, *442*, 275–287. [CrossRef]
9. Asseli, R.; Benaicha, M.; Derbal, S.; Allam, M.; Dilmi, O. Electrochemical Nucleation and Growth of Zn-Ni Alloys from Chloride Citrate-Based Electrolyte. *J. Electroanal. Chem.* **2019**, *847*, 113261. [CrossRef]
10. Feng, Z.; Li, Q.; Zhang, J.; Yang, P.; Song, H.; An, M. Electrodeposition of Nanocrystalline Zn–Ni Coatings with Single Gamma Phase from an Alkaline Bath. *Surf. Coat. Technol.* **2015**, *270*, 47–56. [CrossRef]
11. Fashu, S.; Gu, C.D.; Wang, X.L.; Tu, J.P. Influence of Electrodeposition Conditions on the Microstructure and Corrosion Resistance of Zn–Ni Alloy Coatings from a Deep Eutectic Solvent. *Surf. Coat. Technol.* **2014**, *242*, 34–41. [CrossRef]
12. Soares, M.E.; Souza, C.A.C.; Kuri, S.E. Characteristics of a Zn–Ni Electrodeposited Alloy Obtained from Controlled Electrolyte Flux with Gelatin. *Mater. Sci. Eng. A* **2005**, *402*, 16–21. [CrossRef]
13. Byk, T.V.; Gaevskaya, T.V.; Tsybulskaya, L.S. Effect of Electrodeposition Conditions on the Composition, Microstructure, and Corrosion Resistance of Zn–Ni Alloy Coatings. *Surf. Coat. Technol.* **2008**, *202*, 5817–5823. [CrossRef]

14. Feng, Z.; Wang, L.; Li, D.; Sun, Q.; Xing, P.; An, M. Electrochemical Studies of 2-Aminopyridine on Nanocrystalline Zn–Ni Alloy Electrodeposition. *J. Electroanal. Chem.* **2019**, *835*, 114–122. [CrossRef]
15. Abedini, B.; Ahmadi, N.P.; Yazdani, S.; Magagnin, L. Structure and Corrosion Behavior of Zn-Ni-Mn/Zn Ni Layered Alloy Coatings Electrodeposited under Various Potential Regimes. *Surf. Coat. Technol.* **2019**, *372*, 260–267. [CrossRef]
16. Oliveira, R.P.; Bertagnolli, D.C.; da Silva, L.; Ferreira, E.A.; Paula, A.S.; da Fonseca, G.S. Effect of Fe and Co Co-Deposited Separately with Zn-Ni by Electrodeposition on ASTM A624 Steel. *Appl. Surf. Sci.* **2017**, *420*, 53–62. [CrossRef]
17. Yang, Z.N.; Zhang, Z.; Zhang, J.Q. Electrodeposition of Decorative and Protective Zn–Fe Coating onto Low-Carbon Steel Substrate. *Surf. Coat. Technol.* **2006**, *200*, 4810–4815. [CrossRef]
18. Swathirajan, S. Electrodeposition of Zinc + Nickel Alloy Phases and Electrochemical Stripping Studies of the Anomalous Codeposition of Zinc. *J. Electroanal. Chem. Interfacial Electrochem.* **1987**, *221*, 211–228. [CrossRef]
19. Ortiz-Aparicio, J.L.; Meas, Y.; Trejo, G.; Ortega, R.; Chapman, T.W.; Chainet, E.; Ozil, P. Electrodeposition of Zinc-Cobalt Alloy from a Complexing Alkaline Glycinate Bath. *Electrochim. Acta* **2007**, *52*, 4742–4751. [CrossRef]
20. Rahman, M.J.; Sen, S.R.; Moniruzzaman, M.; Shorowordi, K.M. Morphology and Properties of Electrodeposited ZN-NI Alloy Coatings on Mild Steel. *J. Mech. Eng.* **1970**, *40*, 9–14. [CrossRef]
21. Gharahcheshmeh, M.H.; Sohi, M.H. Study of the Corrosion Behavior of Zinc and Zn–Co Alloy Electrodeposits Obtained from Alkaline Bath Using Direct Current. *Mater. Chem. Phys.* **2009**, *117*, 414–421. [CrossRef]
22. Nayana, K.O.; Venkatesha, T.V.; Chandrappa, K.G. Influence of Additive on Nanocrystalline, Bright Zn–Fe Alloy Electrodeposition and Its Properties. *Surf. Coat. Technol.* **2013**, *235*, 461–468. [CrossRef]
23. Brenner, A. Electrodeposition of Alloys: PRINCIPLES and PRACTICE. In *Electrodeposition of Alloys*; Elsevier: Amsterdam, The Netherlands, 1963; Volume I, p. ii. ISBN 9781483223117.
24. Roventi, G.; Cecchini, R.; Fabrizi, A.; Bellezze, T. Electrodeposition of Nickel-Zinc Alloy Coatings with High Nickel Content. *Surf. Coat. Technol.* **2015**, *276*, 1–7. [CrossRef]
25. Bahadormanesh, B.; Ghorbani, M. Electrodeposition of Zn–Ni–P Compositionally Modulated Multilayer Coatings: An Attempt to Deposit Ni–P and Zn–Ni Alloys from a Single Bath. *Electrochem. Commun.* **2017**, *81*, 93–96. [CrossRef]
26. Li, R.; Dong, Q.; Xia, J.; Luo, C.; Sheng, L.; Cheng, F.; Liang, J. Electrodeposition of Composition Controllable Zn Ni Coating from Water Modified Deep Eutectic Solvent. *Surf. Coat. Technol.* **2019**, *366*, 138–145. [CrossRef]
27. Miranda, F.J.F.; Barcia, O.E.; Diaz, S.L.; Mattos, O.R.; Wiart, R. Electrodeposition of Zn-Ni Alloys in Sulfate Electrolytes. *Electrochim. Acta* **1996**, *41*, 1041–1049. [CrossRef]
28. Hammami, O.; Dhouibi, L.; Triki, E. Influence of Zn–Ni Alloy Electrodeposition Techniques on the Coating Corrosion Behaviour in Chloride Solution. *Surf. Coat. Technol.* **2009**, *203*, 2863–2870. [CrossRef]
29. Hegde, A.C.; Venkatakrishna, K.; Eliaz, N. Electrodeposition of Zn-Ni, Zn-Fe and Zn-Ni-Fe Alloys. *Surf. Coat. Technol.* **2010**, *205*, 2031–2041. [CrossRef]
30. Albalat, R.; Gómez, E.; Müller, C.; Sarret, M.; Vallés, E.; Pregonas, J. Electrodeposition of Zinc-Nickel Alloy Coatings: Influence of a Phenolic Derivative. *J. Appl. Electrochem.* **1990**, *20*, 635–639. [CrossRef]
31. Maciej, A.; Wadas, A.; Sowa, M.; Socha, R.; Dercz, G.; Rabe, M.; Simka, W. Improvement of Corrosion Resistance of Zn-Ni Alloy Coatings by Anodizing in Selected Alcoholic Solutions. *Corros. Sci.* **2019**, *158*, 108107. [CrossRef]
32. Kwon, M.; Jo, D.h.; Cho, S.H.; Kim, H.T.; Park, J.T.; Park, J.M. Characterization of the Influence of Ni Content on the Corrosion Resistance of Electrodeposited Zn-Ni Alloy Coatings. *Surf. Coat. Technol.* **2016**, *288*, 163–170. [CrossRef]
33. Pouladi, S.; Shariat, M.H.; Bahrololoom, M.E. Electrodeposition and Characterization of Ni-Zn-P and Ni-Zn-P/Nano-SiC Coatings. *Surf. Coat. Technol.* **2012**, *213*, 33–40. [CrossRef]
34. Mosavat, S.H.; Bahrololoom, M.E.; Shariat, M.H. Electrodeposition of Nanocrystalline Zn-Ni Alloy from Alkaline Glycinate Bath Containing Saccharin as Additive. *Appl. Surf. Sci.* **2011**, *257*, 8311–8316. [CrossRef]
35. Anwar, S.; Khan, F.; Zhang, Y. Electrochemical Analysis of an Electrodeposited Zn-Ni Alloy Films Contained EDTA Stable Baths in 3.5 Wt% NaCl Solutions. *Mater. Today Proc.* **2020**, *28*, 532–537. [CrossRef]
36. Ghaziof, S.; Gao, W. Electrodeposition of Single Gamma Phased Zn–Ni Alloy Coatings from Additive-Free Acidic Bath. *Appl. Surf. Sci.* **2014**, *311*, 635–642. [CrossRef]
37. Fashu, S.; Gu, C.D.; Zhang, J.L.; Huang, M.L.; Wang, X.L.; Tu, J.P. Effect of EDTA and NH4Cl Additives on Electrodeposition of Zn-Ni Films from Choline Chloride-Based Ionic Liquid. *Trans. Nonferrous Met. Soc. China* **2015**, *25*, 2054–2064. [CrossRef]
38. Bahadormanesh, B.; Ghorbani, M. Ni-P/Zn-Ni Compositionally Modulated Multilayer Coatings—Part 2: Corrosion and Protection Mechanisms. *Appl. Surf. Sci.* **2018**, *442*, 313–321. [CrossRef]
39. Ataie, S.A.; Zakeri, A. RSM Optimization of Pulse Electrodeposition of Zn-Ni-Al2O3 Nanocomposites under Ultrasound Irradiation. *Surf. Coat. Technol.* **2019**, *359*, 206–215. [CrossRef]
40. Oliveira, J.A.M.; de Almeida, A.F.; Campos, A.R.N.; Prasad, S.; Alves, J.J.N.; de Santana, R.A.C. Effect of Current Density, Temperature and Bath PH on Properties of Ni–W–Co Alloys Obtained by Electrodeposition. *J. Alloys Compd.* **2021**, *853*, 157104. [CrossRef]
41. Oliveira, A.L.M.; Costa, J.D.; De Sousa, M.B.; Alves, J.J.N.; Campos, A.R.N.; Santana, R.A.C.; Prasad, S. Studies on Electrodeposition and Characterization of the Ni-W-Fe Alloys Coatings. *J. Alloys Compd.* **2015**, *619*, 697–703. [CrossRef]
42. Costa, J.D.; de Sousa, M.B.; Lia Fook, N.C.M.; Alves, J.J.N.; de Araújo, C.J.; Prasad, S.; Campos, A.R.N.; de Santana, R.A.C. Obtaining and Characterization of Ni-Ti/Ti-Mo Joints Welded by TIG Process. *Vacuum* **2016**, *133*, 58–69. [CrossRef]

43. Costa, J.D.; de Sousa, M.B.; Alves, J.J.N.; Evaristo, B.d.O.; Queiroga, R.A.; dos Santos, A.X.; Maciel, T.M.; Campos, A.R.N.; de Santana, R.A.C.; Prasad, S. Effect of Electrochemical Bath Composition on the Preparation of Ni-W-Fe-P Amorphous Alloy. *Int. J. Electrochem. Sci.* **2018**, *13*, 2969–2985. [CrossRef]
44. Hafeez, A.; Ammar Taqvi, S.A.; Fazal, T.; Javed, F.; Khan, Z.; Amjad, U.S.; Bokhari, A.; Shehzad, N.; Rashid, N.; Rehman, S.; et al. Optimization on Cleaner Intensification of Ozone Production Using Artificial Neural Network and Response Surface Methodology: Parametric and Comparative Study. *J. Clean. Prod.* **2020**, *252*, 119833. [CrossRef]
45. Hosseinpour, M.; Soltani, M.; Noofeli, A.; Nathwani, J. An Optimization Study on Heavy Oil Upgrading in Supercritical Water through the Response Surface Methodology (RSM). *Fuel* **2020**, *271*, 117618. [CrossRef]
46. Heydari, H.; Akbari, M. Investigating the Effect of Process Parameters on the Temperature Field and Mechanical Properties in Pulsed Laser Welding of Ti6Al4V Alloy Sheet Using Response Surface Methodology. *Infrared Phys. Technol.* **2020**, *106*, 103267. [CrossRef]
47. Moreno Dávila, I.M.M.; Tamayo Ordoñez, M.C.; Morales Martínez, T.K.; Soria Ortiz, A.I.; Gutiérrez Rodríguez, B.; Rodríguez de la Garza, J.A.; Ríos González, L.J. Effect of Fermentation Time/Hydraulic Retention Time in a UASB Reactor for Hydrogen Production Using Surface Response Methodology. *Int. J. Hydrogen Energy* **2020**, *45*, 13702–13706. [CrossRef]
48. Ali, A.N.; Huang, S.J. Ductile Fracture Behavior of ECAP Deformed AZ61 Magnesium Alloy Based on Response Surface Methodology and Finite Element Simulation. *Mater. Sci. Eng. A* **2019**, *746*, 197–210. [CrossRef]
49. Abu-Sharkh, S.; Doerffel, D. Rapid Test and Non-Linear Model Characterisation of Solid-State Lithium-Ion Batteries. *J. Power Sources* **2004**, *130*, 266–274. [CrossRef]
50. Yan, M.; Wang, J.; Han, E.; Ke, W. Local Environment under Simulated Disbonded Coating on Steel Pipelines in Soil Solution. *Corros. Sci.* **2008**, *50*, 1331–1339. [CrossRef]
51. Santana, R.A.C.d.; Campos, A.R.N.; Prasad, S.; Leite, V.D. Otimização Do Banho Eletrolítico Da Liga Fe-WB Resistente à Corrosão. *Quim. Nova* **2007**, *30*, 360–365. [CrossRef]
52. Qiao, X.; Li, H.; Zhao, W.; Li, D. Effects of Deposition Temperature on Electrodeposition of Zinc-Nickel Alloy Coatings. *Electrochim. Acta* **2013**, *89*, 771–777. [CrossRef]
53. Tuaweri, T.J. Zn-Ni Electrodeposition for Enhanced Corrosion Performance. *Int. J. Mater. Sci. Appl.* **2013**, *2*, 221. [CrossRef]
54. Hammami, O.; Dhouibi, L.; Berçot, P.; Rezrazi, E.M. Effect of Phosphorus Doping on Some Properties of Electroplated Zn–Ni Alloy Coatings. *Surf. Coat. Technol.* **2013**, *219*, 119–125. [CrossRef]
55. Constantin, I. Microstructural Characterization and Corrosion Behavior of Electroless Ni-Zn-P Thin Films. *J. Metall.* **2014**, *2014*, 827393. [CrossRef]
56. Zheng, Z.; Li, N.; Wang, C.Q.; Li, D.Y.; Meng, F.Y.; Zhu, Y.M. Effects of CeO_2 on the Microstructure and Hydrogen Evolution Property of Ni-Zn Coatings. *J. Power Sources* **2013**, *222*, 88–91. [CrossRef]
57. Mosavat, S.H.; Shariat, M.H.; Bahrololoom, M.E. Study of Corrosion Performance of Electrodeposited Nanocrystalline Zn-Ni Alloy Coatings. *Corros. Sci.* **2012**, *59*, 81–87. [CrossRef]
58. Abou-Krisha, M.M.; Rageh, H.M.; Matter, E.A. Electrochemical Studies on the Electrodeposited Zn-Ni-Co Ternary Alloy in Different Media. *Surf. Coat. Technol.* **2008**, *202*, 3739–3746. [CrossRef]
59. Brenner, A.; Couch, D.E.; Williams, E.K. Electrodeposition of Alloys of Phosphorus with Nickel or Cobalt. *J. Res. Natl. Bur. Stand.* **1950**, *44*, 109. [CrossRef]
60. MacIej, A.; Nawrat, G.; Simka, W.; Piotrowski, J. Formation of Compositionally Modulated Zn-Ni Alloy Coatings on Steel. *Mater. Chem. Phys.* **2012**, *132*, 1095–1102. [CrossRef]
61. Chang, L.M.; Chen, D.; Liu, J.H.; Zhang, R.J. Effects of Different Plating Modes on Microstructure and Corrosion Resistance of Zn–Ni Alloy Coatings. *J. Alloys Compd.* **2009**, *479*, 489–493. [CrossRef]
62. Gnanamuthu, R.; Mohan, S.; Saravanan, G.; Lee, C.W. Comparative Study on Structure, Corrosion and Hardness of Zn–Ni Alloy Deposition on AISI 347 Steel Aircraft Material. *J. Alloys Compd.* **2012**, *513*, 449–454. [CrossRef]
63. Kumar, C.M.; Kumar, P.; Venkatesha, T.V.; Vathsala, K.; Nayana, K.O. Electrodeposition and Corrosion Behavior of Zn-Ni and Zn-Ni-Fe 2O3 Coatings. *J. Coat. Technol. Res.* **2012**, *9*, 71–77. [CrossRef]
64. Tafreshi, M.; Allahkaram, S.R.; Farhangi, H. Comparative Study on Structure, Corrosion Properties and Tribological Behavior of Pure Zn and Different Zn-Ni Alloy Coatings. *Mater. Chem. Phys.* **2016**, *183*, 263–272. [CrossRef]
65. Tozar, A.; Karahan, I.H. Structural and Corrosion Protection Properties of Electrochemically Deposited Nano-Sized Zn-Ni Alloy Coatings. *Appl. Surf. Sci.* **2014**, *318*, 15–23. [CrossRef]
66. Sriraman, K.R.; Brahimi, S.; Szpunar, J.A.; Osborne, J.H.; Yue, S. Characterization of Corrosion Resistance of Electrodeposited Zn-Ni Zn and Cd Coatings. *Electrochim. Acta* **2013**, *105*, 314–323. [CrossRef]
67. Li, S.; Zhang, X.; Zheng, S.; Duan, S.; Cui, J.; Zhang, H. NaHCO3/Na2CO3 as an Inhibitor of Chloride-Induced Mild Steel Corrosion in Cooling Water: Electrochemical Evaluation. *J. Ind. Eng. Chem.* **2021**, *95*, 235–243. [CrossRef]
68. Mishra, P.; Yavas, D.; Bastawros, A.F.; Hebert, K.R. Electrochemical Impedance Spectroscopy Analysis of Corrosion Product Layer Formation on Pipeline Steel. *Electrochim. Acta* **2020**, *346*, 136232. [CrossRef]
69. De Motte, R.; Basilico, E.; Mingant, R.; Kittel, J.; Ropital, F.; Combrade, P.; Necib, S.; Deydier, V.; Crusset, D.; Marcelin, S. A Study by Electrochemical Impedance Spectroscopy and Surface Analysis of Corrosion Product Layers Formed during CO2 Corrosion of Low Alloy Steel. *Corros. Sci.* **2020**, *172*, 108666. [CrossRef]

70. Lukács, Z.; Kristóf, T. A Generalized Model of the Equivalent Circuits in the Electrochemical Impedance Spectroscopy. *Electrochim. Acta* **2020**, *363*, 137199. [CrossRef]
71. Costa, J.D.; Sousa, M.B.; Almeida, A.F.; Oliveira, J.A.M.; Silva, P.C.S.; Alves, J.J.N.; Campos, A.R.N.; Araújo, C.J.; Santana, R.A.C.; Delgado, J.M.P.Q.; et al. Thermal, Mechanical, and Electrochemical Characterization of Ti50Ni50−XMox Alloys Obtained by Plasma Arc Melting. *Metals* **2023**, *13*, 1637. [CrossRef]
72. Silva, C.R.P.; Costa, J.D.; de Almeida, A.F.; Santana, R.A.C.; Campos, A.R.N.; Alves, J.J.N.; Abreu Santos, T.F. Chemical composition variation of the Ni–W alloy as a function of parameters used in the electrodeposition process. *J. Appl. Electrochem.* **2023**. [CrossRef]

Disclaimer/Publisher's Note: The statements, opinions and data contained in all publications are solely those of the individual author(s) and contributor(s) and not of MDPI and/or the editor(s). MDPI and/or the editor(s) disclaim responsibility for any injury to people or property resulting from any ideas, methods, instructions or products referred to in the content.